

Quantum interference of Rydberg excitons in Cu₂O: quantum beats.

Sylwia Zielińska-Raczyńska and David Ziemkiewicz*

Department of Physics, Technical University of Bydgoszcz,

Al. Prof. S. Kaliskiego 7, 85-789 Bydgoszcz, Poland

(Dated: February 25, 2025)

A density matrix formalism is employed to calculate the emission of multi-level excitonic system, highlighting picosecond-scale dynamics and coherent effects such as quantum beats. The results are compared with recent experimental results and indicate some directions of further study. In particular, the effect of Rydberg blockade on the quantum beat phenomenon is discussed.

I. INTRODUCTION

Bound states of electron-hole pairs in semiconductors demonstrate a hydrogen-like behavior in their high-lying excited states that are known as Rydberg excitons (REs). The first observation of those quasiparticles in Cu₂O in 2014 has opened a branch of semiconductor Rydberg physics, which however differs from their atomic analogue due to specific solid state environment; excitons are embedded in the background of a crystal lattice, which interact via screening and scattering.

Rydberg excitons have exaggerated usual excitonic properties including dipole-dipole interactions that scale as n^4 and radiative lifetimes that scale as n^3 exceeding nanoseconds. For highly-excited states with principal quantum number $n >> 1$ the average electron-hole separation can reach μm . They demonstrate strong Kerr type nonlinearities for both visible light ([1],[2]) and for microwaves ([3], [4]). Significant feature of Rydberg excitons is Rydberg blockade, which is a result of a long-range dipole-dipole and van der Waals interactions between them that can be large enough to perturb the energy level of nearby excitons, so they no longer have the same frequency, which prevents their excitation in the immediate vicinity of already existing exciton. So far the static spectroscopic properties of REs have been throughout examined in bulk and in nanoscale systems [5] proving their ability to be viable candidates for quantum technology. Plurality of REs states in copper oxide offers the wealth of available quantum (one or two-photon) excitations in the wide range of frequencies from micro to optical and offers huge amount of dynamical processes which can be studied in REs media. Therefore it seems appropriate to look at Rydberg excitons in the context of their interaction with light and application of their extraordinary properties to different processes involved in the dynamical manipulations of optical processes in which they are involved.

In general, light-matter interaction leads to interesting and relevant coherent and incoherent phenomena which are fundamental to probe the properties of materials. Studies based on such interaction have revealed a plethora of information concerning excited quantum

states, their coupling and dynamical time scales associated with fundamental processes in materials (for Cu₂O see [6–8]).

One of coherent effects caused by such interaction is coherent excitonic beats, which is an important spectroscopic signature providing information about excited quantum states. The phenomenon of quantum beating relies on the concept of quantum mechanical superposition of closely-lying excitonic states coupled by a near-resonant laser pulse transition from a ground state [9]. The coherence of two or more excited states that is created by a short laser pulse manifests itself by modulation of the emitted radiation intensity.

Quantum beats have been observed for the first time in 1955 [10]. Recently, experiments with quantum beats can be performed even on single photons demonstrating tunable Hong-Ou-Mandel interference in which the quantum beat of single photons is observed [11].

The observation of quantum beats yields a very direct information about the coherence properties of electronic or vibronic excitations, as was shown for atoms and molecules in many experiments [12, 13] as well for 1S excitonic states [14] and quadrupole polaritons in Cu₂O [15]. They have become an important scientific tool for observing the time evolution of closely spaced energy levels [16]. This makes them particularly well suited for the study of Rydberg excitons.

Grunwald et al [17] have analyzed the quantum coherent properties of Rydberg excitons absorption spectrum in Cu₂O and noticed the role of coherences between two adjacent upper excitonic states. Now Rydberg excitons explorations in Cu₂O have reached a stage at which coherent quantum effects are observed ([18],[19]). This allows for a controlled quantum manipulation and state generation for excitons and opens up the possibility for developing semiconductor quantum technologies. As it was mentioned, Cu₂O provides the flexibility to operate at various frequencies creating Rydberg excitons and separation between Rydberg levels is not much greater than the linewidth of these levels therefore it seems to be suitable medium for realizing quantum beats. This phenomenon reflects an intrinsic quantum mechanical interference and can be applied to Rydberg excitonic physics providing detail insight into the nature of excited states coupling.

In this paper we present the results of the time-

* david.ziemkiewicz@utp.edu.pl

dependent behavior of Rydberg excitons excited by a short laser pulse leading to creation of quantum beats. Our calculations based on the master equation [20], in which quantum coherences are represented by off-diagonal elements of the density matrix. In Sec. II we set up the formalism for coherent exciton-state generation by the pump pulse. Next, in Sec. III we apply presented equations to calculate the different cases of one- and two-photon excitations of Rydberg excitons in Cu_2O and emission of quantum beats in various configurations. Sec. IV is devoted to the analysis of Rydberg blockade influence on quantum beats spectra. Finally, we summarize our conclusions in Sec. V. Two Appendices contain calculation of dipole/quadrupole matrix elements and estimation of exciton density.

II. THEORY

Excitons are hydrogen-like excitations and in spite of the dependence of exciton energy on wavevector they may be considered as two-level systems (with a multiple excited state due to degeneracy). This is because in the absorption process energy and wavevector are conserved so the resonant excitation with light will create the exciton in a state with well-defined energy and \mathbf{k} . Here we focus our interest on the dynamical aspects and properties of Rydberg excitons in Cu_2O . We will show that due to interaction with a laser pulse Rydberg excitonic states can be used to create the quantum collective beats, which are the outcome of a superposition between at least two different energy levels. Quantum beats are manifested in the oscillating and decaying of radiation emitted by the system. These oscillations are the result of emission from a superposition of excited states created by off-resonant excitation.

We consider a system presented on Fig. 1, it consists of valence band as a ground state which is coupled to at least two (or more) upper Rydberg excitonic states by non resonant laser pulse. A single exciton resonance is modeled by two states, the excited state $|j\rangle$ and the excitonic vacuum as a ground state. Both states are coupled by the laser pulse of frequency ω , amplitude ε and polarization \mathbf{e}

$$\mathbf{E}(z, t) = \mathbf{e}\varepsilon(z, t) \exp[i(\omega t - kz)]$$

is short and spectrally wide so it can couple all upper states at the same time, see Fig. 1.

The time evolution of the excitonic density matrix $\rho = \rho(z, t)$ for an exciton at position z is described by von Neumann equation with a dissipative term [20]

$$i\hbar\dot{\rho} = [H, \rho] + R\rho. \quad (1)$$

The Hamiltonian of such a system interacting with an

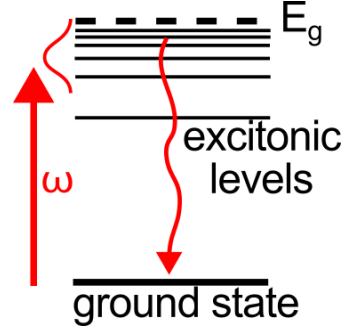


FIG. 1: General schematic of the system.

electromagnetic wave has the form

$$H = H_0 + V + H_{vdW} = E_a|a\rangle\langle a| + \sum_j E_j|j\rangle\langle j| + \sum_j 2\Omega_j \cos(\omega t)[|a\rangle\langle j| + |j\rangle\langle a|] + H_{vdW}, \quad (2)$$

where $\Omega_j = \frac{\varepsilon d_{aj}}{2\hbar}$ is the Rabi frequency for the $a \rightarrow j$ transition. In Rydberg systems the dipole-dipole interaction between excitons is responsible for reduction of absorption, because of energy levels shifting and it manifested in so-called Rydberg blockade [21], where a resonant excitation of another exciton in a vicinity to the same Rydberg state is prevented and an absorption bleaching is observed. The influence of Rydberg blockade results in strongly correlated many-body states of Rydberg excitations [22], and is described by a van der Waals potential in the form

$$H_{vdW} = \sum_{\mu} \frac{C_6^{\mu}}{R_{ij}^6} |\mu\rangle\langle\mu| \quad (3)$$

where $|\mu\rangle$ is a two-exciton eigenstate [23]. It should be mentioned that particularly for excitonic states with high principal quantum number n the influence of the blockade is considerable since coefficient $C_6 \sim n^{11}$, so that the van der Waals interaction leads to a significant shift of exciton energetic levels. However, the number of created excitons depends on the laser intensity, therefore for lower excitons induced by rather low laser intensities the blockade effect can be negligible, while for high excitonic states Rydberg blockade is present even for a very low laser power.

To illustrate and specify a theoretical approach we restrict our model to three-level system: valence band a and two arbitrary upper excitonic states b and c . After making the rotating-wave approximation, i.e., transforming-off the terms oscillating rapidly with optical frequency factors: $\rho_{aj} = \sigma_{aj} e^{i\omega t}$, $\rho_{aa} = \sigma_{aa}$, $\rho_{jj} = \sigma_{jj}$ and adding terms describing relaxations within the sys-

tem, von Neumann equation can be written in the form

$$\begin{aligned}
i\dot{\sigma}_{aa} &= V_{ab}\sigma_{ba} + V_{ac}\sigma_{ca} - V_{ba}\sigma_{ab} - V_{ca}\sigma_{ac} \\
&\quad + i\Gamma_{ba}\sigma_{bb} + i\Gamma_{ca}\sigma_{cc} \\
i\dot{\sigma}_{bb} &= V_{ba}\sigma_{ab} - V_{ab}\sigma_{ba} - i\Gamma_{ba}\sigma_{bb} + i\Gamma_{cb}\sigma_{cc} \\
i\dot{\sigma}_{cc} &= V_{ca}\sigma_{ac} - V_{cb}\sigma_{ca} - i\Gamma_{ca}\sigma_{cc} + i\Gamma_{cb}\sigma_{cc} \\
i\dot{\sigma}_{ab} &= (E_a + \omega - E_b)\sigma_{ab} + V_{ab}\sigma_{bb} + V_{ac}\sigma_{cb} \\
&\quad - V_{ab}\sigma_{aa} - i\gamma_{ab}\sigma_{ab} \\
i\dot{\sigma}_{ac} &= (E_a + \omega - E_c)\sigma_{ac} + V_{ac}\sigma_{cc} + V_{ab}\sigma_{bc} \\
&\quad - V_{ac}\sigma_{aa} - i\gamma_{ac}\sigma_{ac} \\
i\dot{\sigma}_{bc} &= (E_b - E_c)\sigma_{bc} + V_{bc}\sigma_{bc} - V_{bc}\sigma_{ba}. \quad (4)
\end{aligned}$$

As mentioned above, for a sufficient pump power, the excitonic energy levels $E_{b,c}$ will be subjected to an energy shift caused by the interaction H_{VdW} . Since the number of excitons in the system is a dynamic quantity, energy levels will also shift in time, adding another layer of complexity to the system dynamics. The topic of Rydberg blockade is discussed in detail in section IV.

The dissipative coefficients $\Gamma_{ij}, i \neq j$ describe a damping of exciton states and are determined by temperature-dependent homogeneous broadening due to phonons [24] and broadening due to eventual impurities or structural imperfections. The relaxation damping rates for coherences are denoted by $\gamma_{ij}, i \neq j$; $\gamma_{ab} = \Gamma_{ba}/2, \gamma_{ac} = \Gamma_{ca}/2$ [25] and the relaxations between upper Rydberg states are neglected. It should be noted that only the relaxations inside the system are considered therefore the total probability is conserved; $\sigma_{aa} + \sigma_{bb} + \sigma_{cc} = 1$ and $\sigma_{aa}(0) = 1$.

In Cu_2O crystal the uppermost valence band has Γ_5^+ symmetry, which is split into a lower band Γ_8^+ and an upper band Γ_7^+ by the spin-orbit interaction, and together with the lowest conduction bands Γ_6^+ and Γ_8^+ results in four exciton series (yellow, green, blue and violet). Due to symmetry properties of valence and conduction bands two types of excitation are possible - dipole allowed (P excitons) and dipole forbidden, but quadrupole allowed (S or D excitons) because of the positive parity of both the conduction and the valence band. For dipole allowed (one-photon) transitions the coupling elements are $V_{ab} = -\varepsilon d_{ab}, V_{ac} = -\varepsilon d_{ac}$, d_{aj} being dipole moment, while for dipole forbidden excitation can be realized by two-photon transition through a virtual non-resonant state v

$$V_{ab} = \frac{W_{av}W_{vb}}{E_a - E_v - \tilde{\omega}}, \quad \tilde{\omega} = \frac{\omega}{2}, \quad (5)$$

where $W_{av} = -\varepsilon d_{av}$.

The mean multipole (dipole or quadrupole) moment M between ground and excited states is given by

$$\begin{aligned}
\langle M \rangle &= Tr\rho M = (\sigma_{ab}M_{ba} + \sigma_{ac}M_{ca})e^{i\omega t} \\
&\quad + (\sigma_{ba}M_{ab} + \sigma_{ca}M_{ac})e^{-i\omega t} \\
&\quad + (\sigma_{bc}M_{cb} + \sigma_{cb}M_{bc}), \quad (6)
\end{aligned}$$

and the time-dependent intensity of an emitted light pulse is proportional to $I(t) \sim |\langle M \rangle|^2$. Due to superposition of upper excited states, contributions of which interfere, the emitted signal is modulated with the oscillation frequency

$$\omega_{ij} = \frac{2\pi}{T_{ij}} = \frac{E_i - E_j}{\hbar}. \quad (7)$$

III. QUANTUM BEATS WITH RYDBERG EXCITONS

In the following subsections we will calculate intensity of the emitted signal solving numerically Eqs (4) and (6). The numerical results of above presented calculation scheme illustrate the response of Rydberg excitons in Cu_2O to a picosecond laser pulse that simultaneously excites a number of Rydberg states. In Eq. (4) there are several parameters that need to be fitted to the properties of a particular excitonic system. First, one has the relaxation factors of the two types: Γ_{ca}, Γ_{ba} corresponding to the transition to the ground state and the Γ_{cb} corresponding to the transition between two excitonic levels. For P excitons the values of $\Gamma_{ja}, j = b, c, \dots$ are adapted from the linewidth data presented in Ref. [21]; for S and D excitons dissipation rates are based on the recent experimental measurement of the exciton lifetimes [18]. The relatively weak inter-excitonic transition rate Γ_{cb} is calculated directly from the transition quadrupole moment, as outlined in Appendix A. The couplings V_{ij} depend on the electric field and the transition dipole or quadrupole moment for the specific transition. Again, these quantities are calculated in Appendix A.

On the other hand, the experimentally measured photoluminescence intensity depends heavily on nonradiative processes [26]. Therefore, we only calculate normalized emission intensity and make no attempt to estimate the absolute value of it, which may depend on many experimental conditions.

In Cu_2O off-resonant coupling to the transitions that promotes an exciton to any upper state provides the flexibility to operate at various frequencies between arbitrary excitonic states, that enables one to analyze at least three cases discussed below. In all considered examples we use realistic pulse laser parameters with the time duration of $\tau = 4$ ps [18] and power density that is sufficiently low that the effects of Rydberg blockade can be neglected; the conditions where blockade is present are discussed in section IV. In each calculation, the central frequency and spectral width of the laser are adjusted to excite the specified excitonic levels. We assume that the spectral width and pulse duration of the laser can be adjusted separately, and at all times the parameters are well above the energy-time uncertainty relation $\Delta E \Delta t \gg \hbar/2$.

A. One-photon excitation

As a first example, we consider a generic situation of a simple 3-level model with a system depicted on Fig. 1, where transition is dipole allowed. The laser spectrum is adjusted so that only $7P$ and $8P$, which are very close to each other (with corresponding energies of $E_{7P} = 2170.182$ meV and $E_{8P} = 2170.635$ meV [21]), are excited and the quantum beats are realized between them. The pulse is covering both upper excitonic levels and excites them simultaneously. The calculation result is shown on Fig. 2. Logarithmic scale is used to show multiple beats clearly; in experimental scenario only a few first oscillations, for $t < 30$ ps, would be visible above the background noise. The energy spacing between these states is thus 0.453 meV which corresponds to the frequency $\omega_{12} \approx 0.7$ THz. Thus, the quantum beat oscillation period is $T \sim 9$ ps. The emitted signal resembles a damped harmonic oscillator with the period T_{ij} , which agrees well with the energy splitting between exciton states. It is worth stressing that such an oscillating behavior is an evident feature of the quantum coherences arising from coherent superposition of excitons. No quantum beats will be observed from any single excitons; they originate only from their coherent superposition.

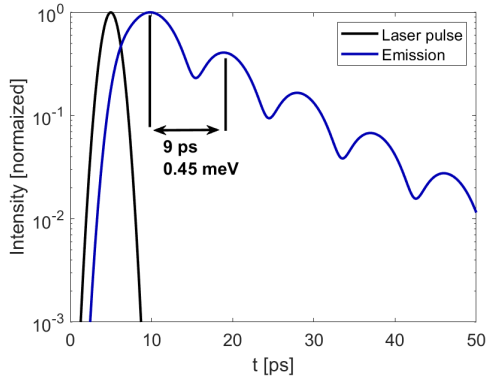


FIG. 2: Normalized emission intensity (in log scale) as a function of time for 7P-8P system.

As it was mentioned above, quantum beat investigations can be extended to a system with several closely spaced transitions, as it is in Rydberg excitons medium. One of the unique features of the recent pulsed laser experiments [18] is the fact that the pulses are relatively wideband, so that they cover majority of the excitonic spectrum. This allows for simultaneous observation of multiple excitonic lines and their complex quantum beat patterns. To model such a situation one has to extend set of Eqs. (4) for more excitons and couplings, accordingly with Eq. (6), which has to be expanded to allow for three P excitons. As in the first case, the laser impulse has a duration of 4 ps but its spectrum is slightly wider to cover the 6P exciton ($E_{6P} = 2169.46$ meV) as well.

The results obtained for such a case are shown on Fig.

3 and show the complicated pattern of multilevel quantum beats. The amplitudes of individual beat frequency

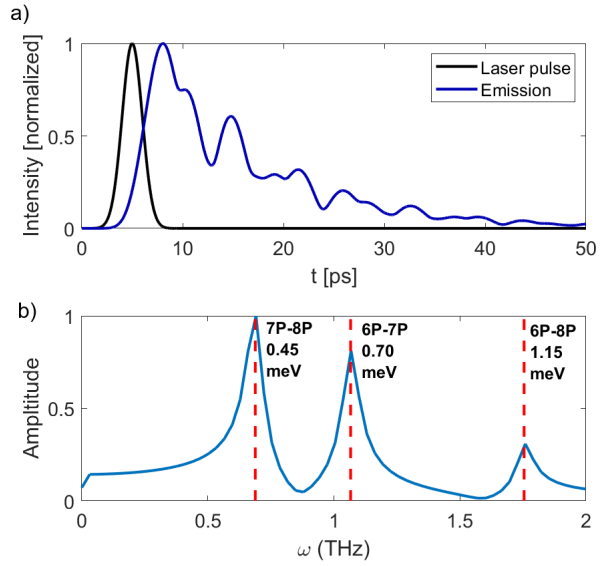


FIG. 3: a) Normalized emission intensity (linear scale) as a function of time for 6P-7P-8P system. b) Frequency spectrum of the emission. Red, dashed lines indicate the individual beats corresponding to 6P-7P, 6P-8P, 7P-8P energy level spacings.

components depend on the relative transition dipole moments of corresponding transitions. One can observe irregular oscillations which are outcome of interference from several beats originating from different superposition of excitonic states. The frequency spectrum of the emitted light is shown on Fig. 3 b). One can notice the frequencies matching the energy separation between nearby states. The dashed lines indicate the individual beats between relevant pairs of excitons.

B. Quantum beats with two-photon excitation

Here, the two-photon excitation enables one to observe quantum beats from levels of the same parity will be analyzed. As a first example, one can consider two states n_1 , n_2 with either S or D excitons (see Fig. 4), the theoretical predictions can be compared with available experimental data. We will analyze a model of emission process similar to the recent experiment in [18], where a set of excitonic states is excited via non resonant virtual level by two-photon absorption of infrared pulses and then, the excitons recombine emitting visible light. Of particular relevance is the case of $n_1 = n_2$, with upper D state and lower S state. Again, the laser pulse is sufficiently spectrally wide to couple to both states at the same time. The numerical calculations of Eqs. (4-6) were performed with the energies of S and D exciton states are taken from [27]. Here, we consider power den-

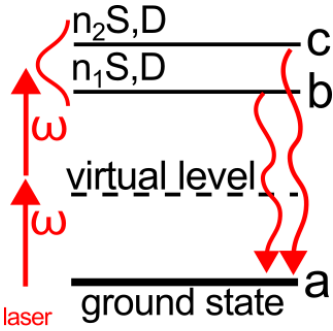


FIG. 4: Schematic of the system approximating the experiment from Ref. [18].

sity for which the Rydberg blockade is weak enough that these energies can be assumed to be fixed; the inclusion of Rydberg blockade mechanism leading to dynamic shift of excitonic levels is discussed in a later section.

The Fig. 5 shows the calculated emission of the $5S-5D$ exciton state pair. An incident laser pulse has a duration

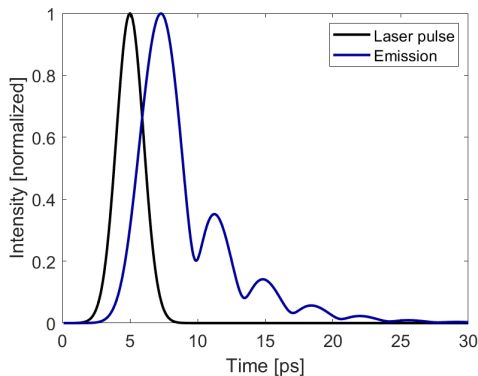


FIG. 5: Normalized emission intensity (linear scale) of $n=5$ S,D excitonic states as a function of time.

of $\tau_L \sim 4$ ps, similarly to the experiment in [18]. The absorption of the laser pulse results in an increase of exciton population, which then decays. However, the emission is not simply proportional to exciton population, but as can be seen from Eq. (4), the emitted signal is a complex function of time-dependent coherences and dipole or quadrupole moments. Specifically, in this particular example the quantum beat oscillations correspond to the $5S \rightarrow 5D$ transition. As expected, the frequency of beats oscillations is in agreement with level separation, which is $E_{5D} - E_{5S} = 0.56$ meV [27], corresponding to $\omega = 0.85$ THz and beat period of 7.3 ps. The general shape of emission, shown here in linear scale, is consistent with experimental results [18].

Similar calculation can be performed for various excitonic states. A comparison of emission intensities of various pairs of S,D exciton states with different principal quantum numbers n is shown on Fig. 6. As expected, the decay of the emission intensity is slower for higher n

due to the longer lifetime. Moreover, because the energy spacing between nS and nD states decreases with n , the frequency ω_{ij} of quantum beats correspondingly declines for highly excited states.

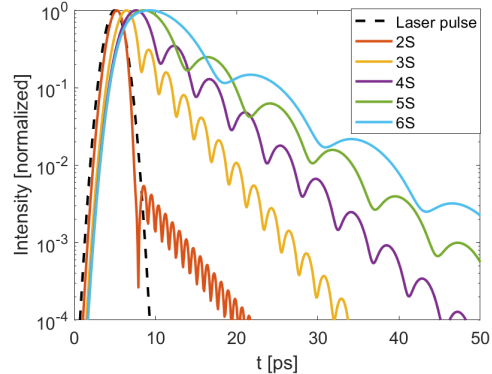


FIG. 6: Comparison of normalized emission intensity (log scale) of pairs of S,D excitonic states with various principal quantum numbers.

C. Emission spectrum of multi-level system

A next step from calculating emission at a single frequency is to calculate the entire spectrum, so that one can follow the evolution of multiple emission lines of the system, similarly to the results presented in [18]. The normalized, single-frequency emission intensities calculated from Eq. (6) are scaled according to the corresponding oscillator strengths [27], describing emission intensity of individual excitonic states. A remarkable feature of Cu_2O is the fact that the D exciton oscillator strength is particularly large, so that both S and D exciton lines are clearly visible in the emission spectrum [14, 28]. We use the Lorentzian shapes of emission lines [28], with linewidths according to recent measurements [18]. The laser is centered on an energy $E_0 = 2165$ meV and has a linewidth of 10 meV, which covers the majority of the exciton spectrum, from $3S$ state to the band gap. The results are shown on Fig. 7. The laser reaches maximum intensity at $t = 10$ ps. The emission intensity (color) reaches maximum slightly later, with the delay increasing with n . As expected, states with larger principal quantum number are characterized by a longer emission time due to their longer lifetimes. In the case of $7S$ and $8S$ states, quantum beats can be discerned at $t=30-60$ ps (Fig. 7 inset). It is worth stressing that our theoretical calculations based on Eqs. (4-6) with application of experimentally measured parameters for REs give the similar emission spectra in time-domain as ones recently published by Chakrabarti *et al* [18], which validates our theoretical approach. Some differences between calculation results and measured spectra result from the lack of noise in calculations and a rough estimation of dipole

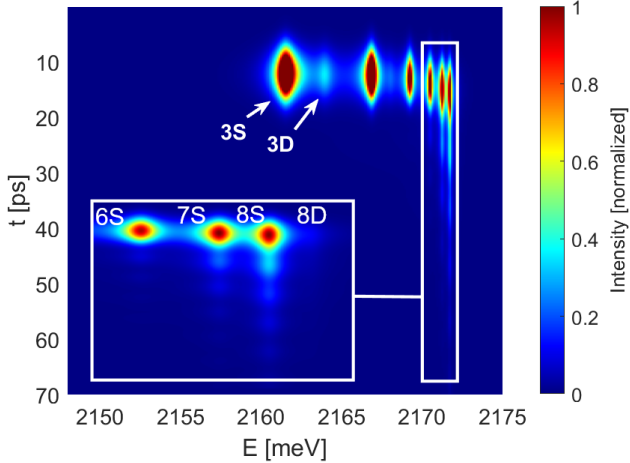


FIG. 7: Emission spectrum as a function of time and energy; inset: a zoom on the 6S-8S lines, highlighting quantum beats.

moments in our approach. It is also not clear if the Rydberg blockade can be completely ignored for $n = 8$, as it was done here, depending on exact peak laser power in experiment.

IV. THE EFFECT OF RYDBERG BLOCKADE

The pump laser power density and duration of the same order as in the recent experiments [18, 29], result in exciton density on the order of $1/\mu\text{m}^3$ [29]. In such conditions, the blockade effects can become nontrivial, especially for highly excited states $n > 10$. We also note that quantum beats are a well-known tool for precisely estimating small spacings between neighboring energy levels, which would be otherwise hard to measure [16]. This is particularly relevant here since even μeV energy level shifts could be feasibly detected in experiments, greatly lowering the power necessary for the blockade effects to become visible.

For the case of P excitons, the so-called blockade volume is given by [21]

$$V_{bl} = 3 \cdot 10^{-7} n^7 \mu\text{m}^3. \quad (8)$$

For $n > 10$, the blockade volume exceeds $3 \mu\text{m}^3$ and the radius exceeds $1 \mu\text{m}$, which means that at this distance, the energy shift caused by Rydberg blockade exceeds the linewidth of the particular state. For a monochromatic source of radiation, this means that further excitons cannot be efficiently created because their absorption lines are too off-resonant. However, in the case of a short, wideband pulse, the excitation is still possible. Therefore, instead of a reduction of absorption, one can possibly observe the shift of excitonic lines directly.

In general, dipole interactions between exciton states characterized by a large quantum number l , such as D excitons, are complex [30], with individual exciton-exciton

interaction energy that can be either positive or negative [31]. This means that various excitonic states can experience redshift or blueshift that depends on the exciton density. For the case of Cu_2O , we follow the blockade potential calculations presented in [23]. The interaction energy between two excitons with quantum number n , located at a distance R_{ij} from each other is described by potential energy

$$V_{ij} = \frac{C_6}{R_{ij}^6}, \quad (9)$$

with the constant $C_6 \sim n^{11}$ that is also dependent on the quantum numbers l_1, l_2 of both excitons [23]. The total energy shift of a given exciton is a sum over its interaction with all other excitons

$$V_i = \sum_{j \neq i} \frac{C_6}{R_{ij}^6}. \quad (10)$$

The total energy of a given exciton is thus $E'_i = E_i + V_i$, where, E_i corresponds to E_b or E_c in Eqs. (4). In order to describe an entire ensemble of excitons, we calculate the average energy shift of the states E_b and E_c . The procedure is as follows: we calculate the absorbed laser power and estimate the total number of excitons N , consistently with Ref. [29], see Appendix B for details. Then, we divide the total population N into populations N_b, N_c proportionally to the density matrix elements σ_{bb}, σ_{cc} . Next step is Monte Carlo simulation [32], where the given numbers of excitons N_b, N_c are distributed randomly in some specified volume. The energy V_i is calculated from Eq. (9) for each exciton and the average is obtained for all excitons with energy level E_b and E_c , leading to average shifted energies E'_b and E'_c .

Apart from Monte Carlo simulation, one can make some simple analytical estimations; assuming that we have N excitons that are distributed evenly in a given volume V , one can calculate the volume per exciton V/N and a corresponding average radius of a sphere \bar{R} . Assuming that these spherical blockade volumes fill the available space using a perfect sphere packing, each sphere has 12 neighbors [33]. This is the approximate number of excitons located within distance \bar{R} of a given exciton. Since the blockade potential falls quickly with \bar{R} , only these nearest neighbors are relevant. Therefore, the total blockade energy can be estimated as

$$V_i \approx 12 \frac{C_6}{\bar{R}^6}, \quad (11)$$

where the exciton density $\rho^{-1} = \frac{4}{3}\pi\bar{R}^3 = \frac{V}{N}$.

For the 3-level systems considered here, one has two distinct excitonic states b, c and three possible interactions $b-c, b-b, c-c$ between different exciton pairs. The total energy shift is calculated as a weighted average of relevant interaction energies, with weights proportional to level populations. For example, let's consider a system from Fig. 4, where levels b and c correspond to $5S$

and 5D exciton. To calculate the energy shift of the 5S exciton, one has to consider S-S and S-D interaction and use the populations of S and D excitons to calculate the weighted average.

The dynamic shifts of various excitonic levels mean that the inter-level energy spacing will change over time, affecting the quantum beats. An example of such an effect is shown on the Fig. 8. The emission intensity ex-

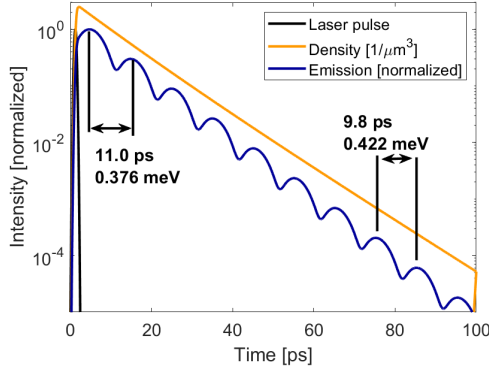


FIG. 8: Emission of the $n=6$ S,D states (in log scale), including the effect of Rydberg blockade. The quantum beat frequency is density-dependent.

hibits a beating pattern with frequency corresponding to the energy spacing between $6S$ and $6D$ states. Initially, when the exciton density is high, this spacing is equal to $E_{6D} - E_{6S} \approx 0.376$ meV. As the population decays, the blockade effect vanishes and energy spacing increases to 0.422 meV. Thus, the blockade-induced energy shift is approximately $\Delta E \approx 46$ μeV. One can conclude that for the power density from [29], a small impact of the Rydberg blockade is already detectable for $n = 6$. Due to the fast n^{11} scaling, the above-mentioned energy shift will exceed the spacing between neighboring S states for $n > 7$. For lower pump power the blockade effect will be correspondingly smaller. Crucially, Fig. 8 illustrates how quantum beats can be used to observe the evolution of blockade-induced energy shifts that are much smaller than the linewidth of the affected excitonic states.

V. CONCLUSIONS

We have presented the method, which based on evolution of density matrix, to calculate the quantum beats in Rydberg excitons medium. Coherent quantum beats are an important phenomenon particularly useful in understanding of coherent light-matter interaction and allowing the observation of coherent quantum effect in Rydberg excitons medium. Quantum beats, which manifest as oscillations in emission intensity, enable one to observe the dynamics of highly excited state transitions in Cu_2O . We should stress that quantum beats are a pure quantum phenomenon, which in case of Rydberg exci-

tons, can be observed for objects of huge (in the quantum scale) dimensions, reaching hundreds of nanometers. We have analyzed several cases of one or two-photon excitations of P , S and D Rydberg excitons, respectively for various excitation frequencies and pulse linewidths. The calculated emission spectra are in good agreement with recent experiments [18]. Crucially, our approach is suitable for modeling quantum beats that are evident in measured spectra. These oscillations, with period given by the inverse transition energy between the excited levels, allows one to precisely measure the separation between levels and observe how it evolves in time. This may be especially useful for possible future studies of Rydberg blockade; unlike traditional, indirect observation of this phenomenon through optical bleaching, quantum beats allow one to measure the blockade-induced energy shifts directly, even in the case where these shifts are much smaller than exciton linewidths.

VI. APPENDIX A: CALCULATION OF DIPOLE AND QUADRUPOLE MOMENTS

Many of the key properties of the excitonic system can be estimated with first-principles calculations using hydrogenlike wavefunctions in the form

$$\Psi_{nlm} = R_{nm}(r)Y_{lm}(\theta, \phi) \quad (12)$$

with

$$R_{nl} = \sqrt{\left(\frac{2}{na^*}\right)^3 \frac{(n-l-1)!}{2n(n+l)!}} e^{-r/na^*} \left(\frac{2r}{na^*}\right)^l L_{n-l-1}^{2l+1} \left(\frac{2r}{na^*}\right) \quad (13)$$

with Bohr radius $a^* = 1.1$ nm and generalized Laguerre polynomial L . The angular part

$$Y_{l,m}(\theta, \phi) = (-1)^m \sqrt{\frac{2l+1}{4\pi} \frac{(l-m)!}{(l+m)!}} P_l^m(\cos(\theta)) e^{im\phi} \quad (14)$$

with associated Legendre polynomial P_l^m .

For the purpose of initial verification of the results, we will follow the experimental data of Kazimierczuk et al [21]. In particular, we assume the same Bohr radius $a^* = 1.1$ nm and other relevant material parameters.

First, one can estimate the transition dipole moment of various inter-excitonic transitions, as well as the transition to the ground state. Specifically, the transition moment is

$$d_{12} = \langle \Psi_{n,l,m} | er | \Psi_{n',l',m'} \rangle = \int_{r=0}^{\infty} R_{nm}^* R_{n'm'} r^2 er dr \int_{\theta=0}^{\pi} \int_{\phi=0}^{2\pi} Y_{l,m}^* Y_{l',m'} \sin \theta d\theta d\phi \quad (15)$$

where \vec{r} is projected onto appropriate axis. For the low angular momentum states (S,P,D excitons), the angular part can be readily calculated analytically; for the radial part, especially in the context of high n states, numerical calculation is used. As a first example, let's consider a radiative transition $P_z \rightarrow S$, $l = 1$, $l' = 0$, $m = m' = 0$, $r_z = r \cos \theta$

$$\int_{\theta=0}^{\pi} \int_{\phi=0}^{2\pi} Y_{10}^* Y_{00} \sin \theta \cos \theta d\theta d\phi = \frac{1}{\sqrt{3}} \quad (16)$$

which is the result used in the work [34]. The table 1 contains the transition dipole moments calculated with the above factor and numerically integrated radial function overlap.

n1S\ n2P	2	3	4	5	6	7	8
1	1.29	0.52	0.30	0.21	0.15	0.12	0.10
2	5.19	3.06	1.28	0.77	0.54	0.41	0.32
3	0.94	12.72	5.46	2.26	1.36	0.95	0.72
4	0.38	2.44	23.21	8.51	3.45	2.06	1.44
5	0.23	0.97	4.60	36.71	12.20	4.86	2.88
6	0.16	0.57	1.79	7.40	53.19	16.54	6.50
7	0.12	0.40	1.04	2.83	10.86	72.67	21.53
8	0.09	0.30	0.72	1.64	4.10	14.96	95.15

TABLE I: Transition dipole moments for $n_1S \rightarrow n_2P$ transitions and various n_1 , n_2 , in multiples of ea^* .

The results are consistent with [35]. As expected, the dipole moment is roughly proportional to exciton size $\sim n^2$ and is the largest for $nS \rightarrow nP$ transition.

Now, we can proceed to calculate the quadrupole transitions necessary for comparison with the recent results in [18]. Specifically, for $D \rightarrow S$ transition $D_{zz} \rightarrow S$, $l = 2$, $l' = 0$, $m = m' = 0$, $r_z = r \cos \theta$, the radial part of wavefunction overlap is

$$\int_{\theta=0}^{\pi} \int_{\phi=0}^{2\pi} Y_{20}^* Y_{00} \sin \theta \cos^2 \theta d\theta d\phi = \frac{2\sqrt{5}}{15} \quad (17)$$

Again, radial parts are calculated numerically. The results are summarized in table 2.

A striking feature of the results is that while quadrupole moments are smaller than dipole moments by a factor of $\sim a^*$, they increase with n more quickly. Therefore, for sufficiently highly excited states, the dynamics of the system can be dominated by quadrupole transitions.

To calculate the transition rates Γ_{ij} used in Eq. (4), we use the Einstein A coefficient for spontaneous emission

$$A_{ij} = \frac{|d_{ij}|^2 \omega_{ij}^3}{3\pi\epsilon_0\epsilon_b\hbar(c/\sqrt{\epsilon_b})^3} \quad (18)$$

n1S\ n2D	3	4	5	6	7	8
1	0.63	0.41	0.29	0.22	0.17	0.14
2	18.99	2.85	0.93	0.41	0.22	0.13
3	51.34	71.13	14.77	6.22	3.49	2.28
4	16.64	193.60	184.81	41.15	18.10	10.46
5	5.07	64.14	506.18	394.78	89.60	39.79
6	2.69	18.35	169.90	1086.58	743.35	169.22
7	1.75	9.39	46.37	367.80	2053.87	1280.47
8	1.28	6.00	23.05	96.84	699.35	3548.75

TABLE II: Transition quadrupole moments for $n_1S \rightarrow n_2D$ transitions and various n_1 , n_2 , in multiples of $e(a^*)^2$.

with $c/\sqrt{\epsilon_b}$ being the speed of light in Cu₂O. Then, we proceed to calculate the B coefficient for stimulated emission

$$B_{ij} = \Gamma_{ij} = \frac{\pi^2 c^3}{\hbar\omega_{ij}^3} A_{ij}. \quad (19)$$

For the quadrupole transition, the corresponding Einstein coefficient is

$$A_{ij}^q = \frac{|q_{ij}|^2 \omega_{ij}^5}{40\pi\epsilon_0\epsilon_b\hbar(c/\sqrt{\epsilon_b})^5} \quad (20)$$

VII. APPENDIX B: ESTIMATION OF EXCITON DENSITY

In order to estimate the relation between input power and exciton density, the efficiency of two-photon excitation process needs to be known. For that, we refer to [29], where a pulse with intensity of 6.1 mW/cm² was applied to excite the dark exciton states in Cu₂O in the sample thickness of 800 μm . Assuming that the pulse is completely absorbed, the average power density is $\rho_P \approx 0.076$ mW/ μm^3 . The pulse duration is $\tau = 2$ ps. The energy density absorbed by the medium is thus $\rho_E = \rho_P\tau \approx 950$ eV/ μm^3 . The exciton density estimated in [29] is $2.5 \cdot 10^{11} \text{ cm}^{-3} = 0.25 \mu\text{m}^{-3}$. Therefore, the volume per single exciton is $4 \mu\text{m}^3$, corresponding to a sphere radius of approximately 1 μm , which is the mean inter-exciton distance [29].

The energy necessary to create one exciton is $E \approx 2.1$ eV. Therefore, to obtain the exciton density of $0.25 \mu\text{m}^{-3}$, one needs energy density of $\rho'_E \approx 0.525$ eV/ μm^3 . By comparing ρ_E and ρ'_E , we get an efficiency

$$\eta = \frac{0.525}{950} = 5.5 \cdot 10^{-4}. \quad (21)$$

Now, we can calculate the exciton density as a function of pump power. It is given by

$$\rho_e = \frac{\eta}{V} \frac{\int_{t=0}^{\tau} P(t) dt}{E_{exc}}, \quad (22)$$

where V is the medium volume absorbing the pulse, $P(t)$ is the pump power, τ is pulse duration and E_{exc} is exciton energy. In the case where exciton lifetime t_{exc} is comparable to pulse duration, one has to use a convolution to get a modified function

$$P'(t) = \int_{-\infty}^{\infty} P(\tau) e^{-(t-\tau)/t_{exc}} d\tau. \quad (23)$$

Given some exciton density ρ_e , the volume per exciton is $V_e = \rho_e^{-1}$ and the radius of equivalent spherical volume is

$$R = \left(\frac{3V_e}{4\pi} \right)^{1/3}. \quad (24)$$

Assuming the blockade potential $V_{VdW} = C_6/R^6$, one can write

$$V_{VdW} = \frac{C_6}{(\frac{3V_e}{4\pi})^2} = \frac{16}{9}\pi^2 C_6 \rho_e^2. \quad (25)$$

Therefore, the energy shift due to Rydberg blockade is proportional to the square of exciton density, which in turn is a product of pump power and duration. The dependence of exciton density on laser intensity, calculated for sample thickness $L = 800 \mu\text{m}$ and pulse duration $\tau = 4 \text{ ps}$, is shown on Fig. 9 a). The Fig. 9 b) depicts the energy shift caused by Rydberg blockade, as a function of intensity. The strong dependence on quantum number n is evident.

[1] S. Zielińska-Raczyńska, G. Czajkowski, K. Karpiński, and D. Ziemkiewicz, *Nonlinear optical properties and self-Kerr effect of Rydberg excitons*, Phys. Rev. B **99**, 245206, (2019).

[2] C. Morin, J. Tignon, J. Mangeney, S. Dhillon, G. Czajkowski, K. Karpiński, S. Zielińska-Raczyńska, D. Ziemkiewicz, and T. Boulier, Phys. Rev. Lett. **129**, 137401 (2022).

[3] L. A. P. Gallagher, Joshua P. Rogers, J. D. Pritchett, R. A. Mistry, D. Pizzey, Ch. S. Adams, M. P. A. Jones, P. Grünwald, V. Walther, Ch. Hodges, W. Langbein, and S. A. Lynch, Phys. Rev. Research 4, 013031 (2022).

[4] J. D. Pritchett, L. A. P. Gallagher, A. Brewin, H. Q. X. Wong, W. Langbein, S. A. Lynch, C. S. Adams, M. P. A. Jones, *Giant microwave-optical Kerr nonlinearity via Rydberg excitons in cuprous oxide*, APL Photonics **1**, 9(3), 031303 (2024).

[5] A. S. Paul, S. K. Rajendran, D. Ziemkiewicz, T. Volz, and H. Ohadi, *Local tuning of Rydberg exciton energies in nanofabricated Cu₂O pillars*, Communications Materials **5**, 43 (2024).

[6] J. Taylor, S. Goswami, V. Walther, M. Spanner, Ch. Simon, and K. Heshami, *Simulation of many-body dynamics using Rydberg excitons*, Quantum Sci. Technol. **7**, 035016 (2022).

[7] N. Naka, I. Akimoto, and M. Shirai, *Free-carrier generation by two-photon resonant excitation to the excitonic states in cuprous oxide*, Phys. Status Solidi B **250**, 9, 1773-1776 (2013).

[8] C. H. Rotteger, C. K. Jarman, M. M. Sobol, S. F. Sutton, and S. G. Sayres, *Sub-picosecond Dynamics of Rydberg Excitons Produced from Ultraviolet Excitation of Neutral Cuprite (Cu₂O) Clusters, n < 13*, The Journal of Physical Chemistry A **128**(39), 8466-8472 (2024).

[9] M. O. Scully, M. S. Zubairy, *Quantum optics*, Cambridge University Press, 2012.

[10] A. T. Forrester, R. A. Gudmundsen, and P. O. Johnson, *Photoelectric Mixing of Incoherent Light*, Phys. Rev. **99**, 1691 (1955).

[11] T. Legero, T. Wilk, M. Hennrich, G. Rempe, and A. Kuhn, *Quantum Beat of Two Single Photons*, Phys. Rev. Lett. **93**, 070503 (2004).

[12] H. Bitto, J. R. Huber, *Molecular quantum beat spec-*

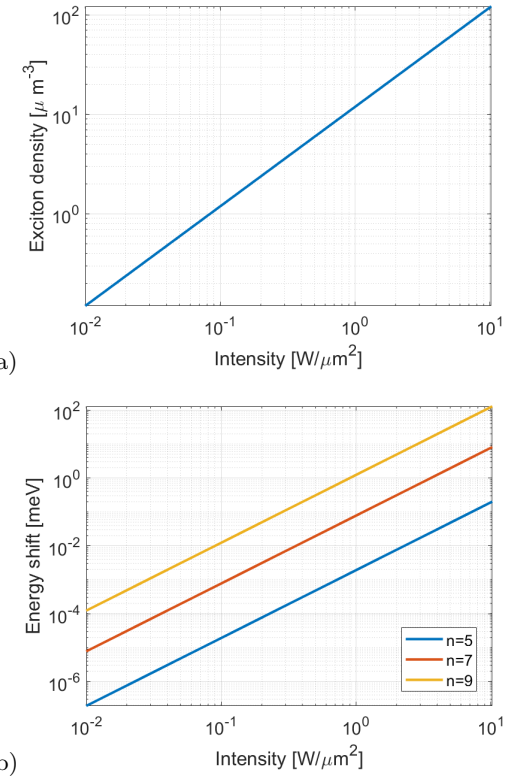


FIG. 9: a) Exciton density as a function of pulse intensity; b) Energy shift as a function of intensity, calculated for S excitons.

troscopy, Optics Communications **80**, 2, 184-198 (1990).

[13] H.S. Han, A.Lee, K. Sinha, F.K. Fatemi, and S. L. Rolston, *Observation of Vacuum-Induced Collective Quantum Beats*, Phys. Rev. Lett. **127**, 073604 (2021).

[14] C. Uihlein, D. Fröhlich, and R. Kenkles, *Investigation of exciton fine structure in Cu₂O*, Phys. Rev. B **23**, 2731 (1981).

[15] D. Fröhlich, A. Kulik, B. Uebbing, A. Mysyrowicz, V.

Langer, H. Stoltz, and W. von der Osten, *Coherent Propagation and Quantum Beats of Quadrupole Polaritons in Cu₂O*, Phys. Rev. Lett. **67**, 17, 2343-2346 (1991).

[16] R. T. Carter and J. R. Huber, *Quantum beat spectroscopy in chemistry*, Chem. Soc. Rev. **29**, 305-314 (2000).

[17] P. Grünwald, M. Assmann, J. Heckötter, D. Fröhlich, M. Bayer, H. Stoltz, and S. Scheel, *Signatures of Quantum Coherences in Rydberg Excitons*, Phys. Rev. Lett. **117**, 133003 (2016).

[18] P. Chakrabarti, K. Morin, D. Lagarde, X. Marie, and T. Boulier, *Direct measurement of the lifetime and coherence time of Cu₂O Rydberg excitons*, arXiv:2410.07355v1 [quant-ph] 9 Oct 2024

[19] K. Orfanakis, S. K. Rajendran, V. Walther, T. Volz, T. Pohl, and H. Ohadi, *Rydberg exciton-polaritons in a Cu₂O microcavity*, Nature Materials **21**, 767-772 (2022).

[20] H. Kondo, Y. Fujimura, and D.S. Lin, *Theory of quantum beats: Master equation approach*, J. Chem. Phys. **75**, 2569-2576, (1981).

[21] T. Kazimierczuk, D. Fröhlich, S. Scheel, H. Stoltz, and M. Bayer, *Giant Rydberg excitons in the copper oxide Cu₂O*, Nature **514**, 344 (2014).

[22] J. Heckötter, V. Walther, S. Scheel, M. Bayer, T. Pohl, M. Assmann, *Asymmetric Rydberg blockade of giant excitons in Cuprous Oxide*, Nat. Commun. **12**, 3556 (2021).

[23] V. Walther, S. Krüger, S. Scheel, and T. Pohl, *Interactions between Rydberg excitons in Cu₂O*, Phys. Rev. B **98**, 165201 (2018).

[24] H. Stoltz, F. Schöne, and D. Semkat, *Interaction of Rydberg excitons in cuprous oxide with phonons and photons: optical linewidth and polariton effect*, New J. Phys. **20**, 023019, (2018).

[25] M. Artoni, J. C. La Rocca, and F. Bassani, *Electromagnetic-induced transparency of Wannier-Mott excitons*, EPL **49** 445 (2000).

[26] M. Takahata, N. Naka, *Photoluminescence properties of the entire excitonic series in Cu₂O*, Phys. Rev. B **98**, 195205 (2018).

[27] F. Schweiner, J. Main, G. Wunner, and C. Uihlein, *Even exciton series in Cu₂O*, Phys. Rev. B **95**, 195201 (2017).

[28] J. P. Rogers, L. A. P. Gallagher, D. Pizzey, J. D. Pritchett, C. S. Adams, M. P. A. Jones, C. Hodges, W. Langbein, and S. A. Lynch, *High-resolution nanosecond spectroscopy of even-parity Rydberg excitons in Cu₂O*, Phys. Rev. B **105**, 115206 (2022).

[29] K. Yoshioka, M. Kuwata-Gonokami, *Dark excitons in Cu₂O crystals for two-photon coherence storage in semiconductors*, Phys. Rev. B **73**, 081202(R) (2006).

[30] M. Assmann, M. Bayer, *Semiconductor Rydberg physics*, Adv. Quantum Technol. **3**, 1900134 (2020).

[31] K. Singer, J. Stanojevic, M. Weidemuller, and R. Cote, *Long-range interactions between alkali Rydberg atom pairs correlated to the ns-ns, np-np and nd-nd asymptotes*, J. Phys. B: At. Mol. Opt. Phys. **38**, 295-307 (2005).

[32] F. Morawetz, S. Sheel, J. Heckötter, M. Assmann, *Many-particle simulation of Rydberg exciton interaction*, Phys. Rev. B **108**, 235205 (2023).

[33] Y. Wu, Z. Fan, and Y. Lu, *Bulk and interior packing densities of random close packing of hard spheres*, Journal of Material Science **38**, 2019-2025 (2003).

[34] D. Ziemkiewicz, S. Zielińska-Raczyńska, *Proposal of tunable Rydberg exciton maser*, Optics Letters **43**, 3742-3745 (2018).

[35] D. Ziemkiewicz, S. Zielińska-Raczyńska, *Solid-state pulsed microwave emitter based on Rydberg excitons*, Optics Express **27**(12), 16983 (2019).